GLOBAL JOURNAL OF PURE AND APPLIED SCIENCES VOL. 6 NO. 3, JUNE 2000:521-536
 ISSN 1118-0579

CROSS SECTION OF EQUATORIAL ELECTROJET MAGNETIC FIELDS

C. AGODI ONWUMECHILI, S. O. OKO and P. O. EZEMA

(Received 6 August 1998; Revision accepted 12 October 1999)

ABSTRACT

In over 2000 traversals across the equatorial electrojet (EEJ) from 1967 to 1969, the POGO series of satellites measured the four-dimensional variation of EEJ magnetic field in certain ranges of local time, altitude, latitude and all longitudes. The enormous quantity of data has been exploited to obtain all the six possible cross sections: longitude-local time, altitude-local time, latitude-local time, altitude-longitude, latitude-longitude and altitude-latitude cross sections for each of the EEJ northward magnetic field, Δx, and downward magnetic field, Δz, most likely for the first time. Each of the four components of the variations is in good agreement with its observations on and near the earth's surface. The landmark values and landmark distances of the component variations as well as the peak values and locations of the contour cells of the cross sections are given. Other interesting features of the cross sections are presented and explained. The physical mechanisms responsible for each of the four components of the variations and therefore for the cross sections are discussed.

Key words: *Magnetic fields of EEJ, latitude-local time cross section, altitude-latitude cross section, longitude-local time cross section.*

1 INTRODUCTION

The equatorial electrojet (EEJ) magnetic fields have been reviewed by Forbush and Casaverde (1961), Onwumechili (1967), Forbes (1981) and Rastogi (1989). The magnetic fields of EEJ vary with local time, altitude, latitude and longitude. The variation is therefore four-dimensional. It is not possible to present the four-dimensional variation in one graph. The approach of this paper is to present the four-dimensional variation in two-dimensional cross sectional slices. Accordingly, each component of EEJ magnetic field has six cross sections, namely: longitude-local time, altitude-local time, latitude-local time, altitude-longitude, latitude-longitude and altitude-latitude cross sections.

Doumouya (1995) has given the latitude-local time cross sections of the magnetic field perturbations of the horizontal (ΔH) and downward vertical (ΔZ) components observed in a chain of stations in West Africa within about ±5° dip latitude across the EEJ. His observed field is the combination of the EEJ and the worldwide part of Sq (WSq) but our presentation here is the EEJ alone. However, his cross sections will be considered in section 10. Apart from Doumouya (1995) we are not aware of any other publication yet of any of the cross sections. Therefore the presentations here may well be the first of their kind.

2 TREATMENT OF DATA

In all the seasons, from 1967-1969, the POGO series of satellites measured the magnetic field of the EEJ in over 2000 traversals across the magnetic dip equator. The measurements covered −30° to 30° dip latitude, all longitudes round the earth, in the altitude range of 400-800 km, from 09 hr to 15 hr local time (Cain and Sweeney 1972, 1973). They therefore provided a vast quantity of EEJ magnetic field data in four-dimensional variation. The objective of this paper is to utilize this unusual quantity of POGO data to present all the six possible cross sections of any one component of EEJ magnetic field.

Onwumechili and Ezema (1992) analyzed the POGO data with a thick current shell model which takes into account the variations in both latitude and altitude. The magnetic field of currents induced in the earth by the external EEJ was represented by the field of an "image" EEJ at a

C. AGODI ONWUMECHILI, 69 Lansdowne Drive, Hackney, London, United Kingdom.
S. O. OKO, Department of Computer Science, University of Nigeria, Nsukka, Nigeria.
P. O. EZEMA, Department of Physics and Astronomy, University of Nigeria, Nsukka, Nigeria

depth of 506 km. Because the EEJ is mainly an eastward current it is usual to ignore the eastward component, Y, of its magnetic field. Therefore, at the time of the analysis in 1990, only the northward X and vertical Z components of its magnetic field and their cross sections were obtained.

Recent developments suggest that the eastward component Y of the EEJ magnetic field may not be altogether negligible at all locations in the EEJ zone. Using the results of the study of quiet time ionospheric currents over the Indian sector (Onwumechili et al. 1996 and Oko et al. 1996), Onwumechili (1996) has produced the current vortex of EEJ. This suggests that the north-south component of the return current of EEJ may produce measurable variations of the declination D where it is greatest at the latitude of EEJ focus. Rastogi (1996) has obtained this ΔD and ΔY of EEJ near the latitude of EEJ focus from the analysis of observed data of Indian stations.

In the thick current shell model used by Onwumechili and Ezema (1992), the formulations of the magnetic field components X and Z needed for our cross sections here are as follows:

(a) For variations with both latitude and altitude:

$$(sg.z)P^4X = \tfrac{1}{2}k\,[1 + \beta)\,(v + \alpha v + 2a)\,(v + a)^2 + (v + \alpha v + 2\,\alpha a)\,(u + \beta u + 3b - \beta b)\,(u + b) + 8(1-\alpha)\,(1-\beta)\,ab(u + b)], \quad \ldots\ldots\ldots\ldots\ldots \quad (1)$$

$$-(sg.\ x)\,P^4Z = \tfrac{1}{2}k[(1 + \alpha)\,(u + \beta u + 2b)\,(u + b)^2 + (u + \beta u + 2\beta b)\,(v + \alpha v + 3a - \alpha a)\,(v + a)] \quad \ldots\ldots\ldots\ldots \quad (2)$$

(b) For variation with latitude on the spherical surface: z = constant

$$(sg.z)P^4X = \tfrac{1}{2}k\,[(1 + \beta)\,(v + \alpha v + 2\,\alpha a)\,(u + b)^2 + 2(1 - \beta)b\,(v + \alpha v + 4a - 2\alpha a)\,(u + b) + (1 + \beta)\,(v + \alpha v + 2a)\,(v + a)^2], \quad \ldots\ldots\ldots\ldots \quad (3)$$

$$-(sg.\ x)\,P^4Z = \tfrac{1}{2}k[(1 + \alpha)\,(1 + \beta)\,(u + b)^3 + (1 + \alpha)\,(1 - \beta)\,b(u + b)^2 + (1 + \beta)\,(v + \alpha v + 3a - \alpha a)(v + a)(u + b). - (1 - \beta)b\,(v + \alpha v + 3a - \alpha a)(v + \alpha)]. \quad \ldots\ldots\ldots\ldots \quad (4)$$

(c) For variation with altitude at constant latitude: x = constant

$$(sg.\ x)\,P^4X = \tfrac{1}{2}k[(1 + \alpha)\,(1 + \beta)\,(v + a)^3 + (1 - \alpha)\,(1 + \beta)\,a(v + a)^2 + (1 + \alpha)\,(u + \beta u + 3b - \beta b)(u + b)(v + a). - (1 - \alpha)a\,(u + \beta u - 5b + 7\beta b)(u + b)]. \quad \ldots\ldots\ldots\ldots \quad (5)$$

$$-(sg.\ x)\,P^4Z = \tfrac{1}{2}k[(1 + \alpha)\,(u + \beta u + 2\beta b)\,(v + \alpha)^2 + 2(1 - \alpha)\,a(u + \beta u + 2\beta b)\,(v + a). + (1 + \alpha)\,(u + \beta u + 2b)(u + b)^2]; \quad \ldots\ldots\ldots\ldots \quad (6)$$

where

origin is at current centre with latitude x northwards and z vertically downwards;

$u = /x/$ and $v = /z/$;

sg. x = sign of x = x/u and is ± 1 when x = 0;

sg. z = sign of z = z/v and is ± 1 when z = 0;

a and b are constant scale distances along x and z respectively;

α and β are dimensionless constants controlling the distribution of current along x and z respectively;

j_o is the peak current density in Akm^{-2} at x = 0 and z = 0;

$k = 0.1\,\pi^2\,abj_o$ is the current constant in Amperes; and $\quad \ldots\ldots\ldots \quad (7)$

$P^2 = (u + b)^2 + (v + a)^2 \quad \ldots\ldots\ldots\ldots\ldots\ldots \quad (8)$

Onwumechili and Ezema (1992) determined the five parameters of the model: j_o, a, α, b and β for the 36 selected longitudes: 0°, 10°, 20°, 30°, ..., 350°E at each of the 7 local time hours: 09, 10,11, 12, 13, 14 and 15 hr for which data were available. Because the height of the current centre cannot be determined from its remote magnetic field, the height of the EEJ was taken from rocket measurements as 106 km. They analyzed 894 profiles of the POGO magnetic data and each profile yielded one value of each parameter. By putting the values of the parameters into any of Eqs. (1) – (6) the appropriate magnetic field can be determined at any point in the meridional plane at a given longitude or local time. For each of the 5 parameters its 894 values are organized into a matrix table of 36 rows for longitudes λ = 0°, 10°, 20°, ..., 350°E and 7 columns for local time hours t = 09, 10, 11, ..., 15 hour. Averaging the rows and columns we also get the daytime mean

values for each of the 36 longitudes and the all longitude mean values for each for the 7 local time hours.

3 DIMENSIONAL COMPONENTS OF THE CROSS SECTIONS

Some of the cross sections look rather complex. However, they can be easily understood and appreciated if the two components making up each of the two-dimensional cross sections are known and are borne in mind. We therefore, start by describing each of the four dimensional components to the variation separately. The physical mechanisms producing them will be covered under the general discussions in section 10.

3.1 Local Time Component

The diurnal variation of equatorial electrojet (EEJ) ΔH intensity is well known. It increases from dawn to a peak around local noon. From the peak the intensity then decreases till dusk when it becomes about as low as at dawn. Examples of the local time variation of EEJ horizontal magnetic field ΔH are in Fig. 2, p. 1849 of Davis et al. (1967), Fig. 9, p.442 of Onwumechili (1967) and Fig. 24. P. 505 of Rastogi (1989).

3.2 Latitudinal Component

The latitudinal profiles of the variations of EEJ ΔX and Δ2 in Fig. 1(a) are obtained by putting the local noon all longitude means of the parameters into Eqs. (3) and (4) respectively. These mean values are: ½k = 16954 Amp., j_o = 10.44 Akm^{-2}; a = 3.37°, α = -1.53, b = 8.84 km, and β = 0.53. The Fig. 1(a) is directly compared with the latitudinal profiles of ΔB_x and ΔB_z in Fig. 1(b) observed by Hesse in Brazil. The observed profiles (solid curves) in Fig. 1 (b) are the combination of the worldwide part of Sq (WSq) shown in broken curves, and the EEJ. Therefore the EEJ in Fig. 1(a) is the equivalent of and is compared with the difference between the solid and the broken curves in Fig. 1 (b).

From a peak near the dip equator, the WSq ΔX (broken curve) decreases monotonically with latitude. But from a peak of ΔX_o at the dip equator the EEJ ΔX decreases to zero in Fig. 1 (a), where the solid and broken curves intersect in Fig. 1(b). This point is the focus of EEJ ΔX at a dip latitude of w_x = 3.6° approximately. It then becomes negative, reaching a minimum value of ΔX_m at a dip latitude of about u_{mx} = 7.5°. This negative EEJ ΔX is caused by the westward return current of EEJ on the flanks of the dip equator. On the combination of the EEJ ΔX and WSq ΔX to get the solid curve in fig. 1(b), the negative EEJ ΔX decreases in magnitude to zero but faster in Fig. 1 (b) than in Fig. 1 (a). The latitudes w_x and u_{mx} from Fig. 1 (a) are in good agreement with those from Fig. 1 (b).

Again, the WSq ΔZ which is ΔB_z in Fig. 1 (b) (broken curve) is not zero at the dip equator but a few degrees to the side of it because the WSq centres at a mean equator about midway between the geographic and the dip equators (Onwumechili et al. 1996). From there the WSq ΔZ increases to the south but decreases to the north to a peak at about 12° dip latitude. At the dip equator the value of EEJ ΔZ denoted by ΔZ_o is virtually zero in Fig. 1 (a) and is equally zero in Fig. 1 (b) where it is the difference between the two intersecting curves. From the dip equator the EEJ ΔZ increases to a peak of ΔZ_M at dip latitude of about u_M = 2.1°. From the latitude u_M, the EEJ ΔZ decreases to zero in Fig. 1 (a), that is where the solid and broken curves intersect in Fig. 1 (b). This is the focus of EEJ ΔZ at a dip latitude of about w_z = 8.1° on the ground. From the latitude w_z, the EEJ ΔZ decreases to a small minimum value ΔZ_m at a dip latitude of about u_{Mz} = 12°. Beyond the latitude U_{mz}, the EEJ ΔZ decreases quickly to zero before 20° dip latitude. It is remarkable that the landmark distances u_M, w_z and u_{Mz} from Fig. 1 (a) derived from the POGO data agree very well with those from the observed profiles in Brazil in Fig. 1 (b).

In addition, the latitudinal profile of WSq ΔZ observed during the International Polar Year in Fig. 7, p. 439, of Onwumechili (1967) is in accord with the WSq ΔZ (broken curve) in Fig. 1 (b). Similarly, the latitudinal profile of ΔZ dominated by EEJ from a Peruvian chain of stations across the EEJ in Fig. 8, p. 440 of Onwumechili (1967) is consistent with the EEJ ΔZ in Fig. 1 (a). Finally, from all the above, observational results on the ground agree very well with the latitudinal profiles of EEJ ΔX and ΔZ derived from the POGO data as given in Fig. 1 (a).

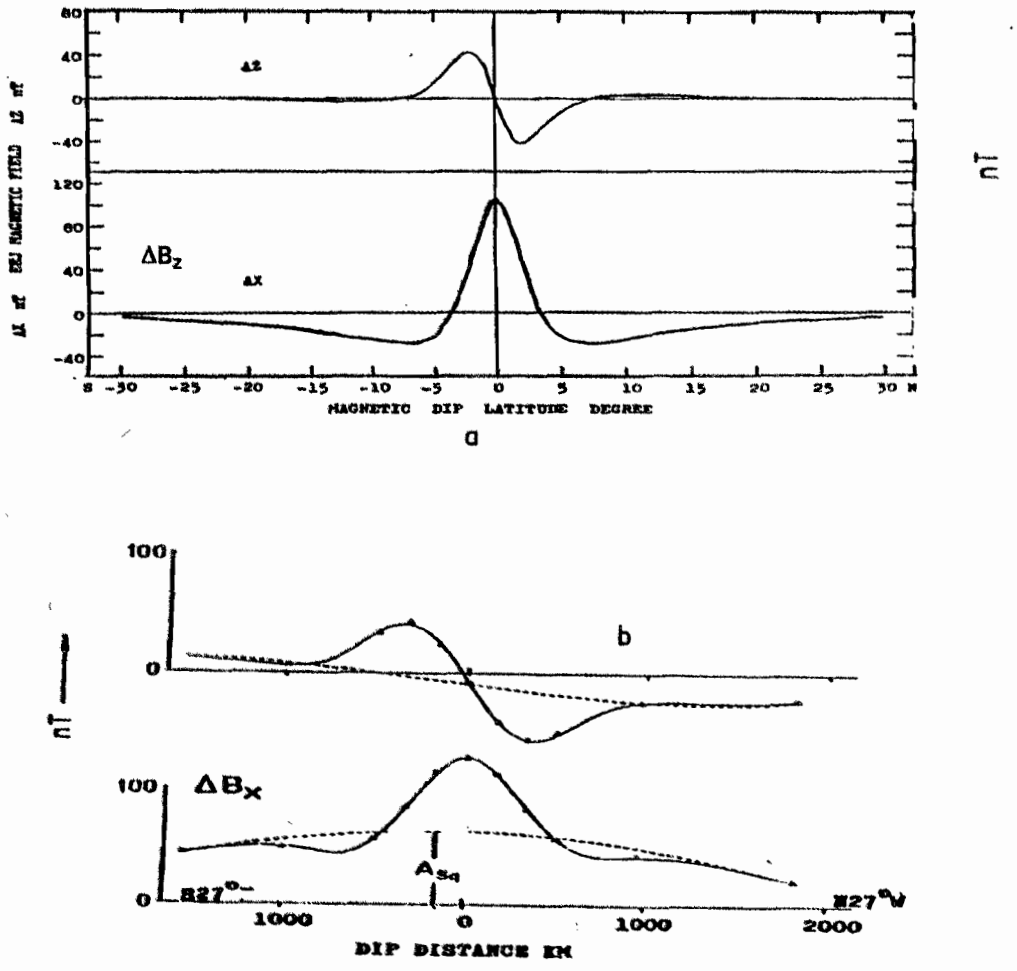

Fig. 1 Latitudinal profiles of northward and downward vertical magnetic fields (external plus internal).
(a) The equatorial electrojet from POGO satellites data based on local noon mean of all longitudes.
(b) The daily ranges observed at a chain of stations across the dip equator in Brazil at 1130 hr LT on 14 November 1971. Solid curve is observed, broken curve is worldwide part of Sq (WSq), and the observed minus WSq is the equatorial electrojet. (Hesse, private communication).

3.3 Altitudinal Component

The EEJ ΔZ is virtually zero at the dip equator. Therefore the vertical variation of ΔX and ΔZ are demonstrated with the fields at 1°S latitude which also makes ΔZ positive. The parameters for all longitude means at local noon, already given in section 3.2, are inserted in Eqs. (5) and (6) for ΔX and ΔZ respectively. In the calculation, u = 1° is constant. The altitude.

$$h = h_e - z = (106 - z) \text{ km}, \quad \ldots\ldots 9$$

where h_e is the altitude of EEJ centre. Although v = /z/, neither ΔX nor ΔZ is symmetrical about the altitude of EEJ centre. Because X changes sign across h_e, the ΔX is the sum of the external and internal fields below h_e but is their difference above h_e. Consequently, the positive peak is larger than the negative peak. Because the internal field continuously decreases with altitude, ΔZ for the same v is slightly smaller below than above h_e.

The resulting altitude profiles of ΔX and ΔZ are given in Fig. 2. Both the positive and negative peaks of ΔX (z) occur at z = 0 because the current is penetrated along the z-axis. These may be compared with the positive and negative peaks of ΔZ (x) which are however apart because the current is not penetrated along the x-axis. After the negative peak at z = 0, the Δx (z) goes through zero to a very negligible maximum at very high altitude similar to Δz_m of Δz (x). From now on we concentrate on the vertical profiles below 1500 km altitude. There is no discontinuity of ΔZ at z = o, h = h_e. Indeed, ΔZ has a maximum at z = 0 similar to the maximum of ΔX at x = 0. Thereafter, ΔZ (z) decreases to zero with increasing altitude as well as with decreasing altitude.

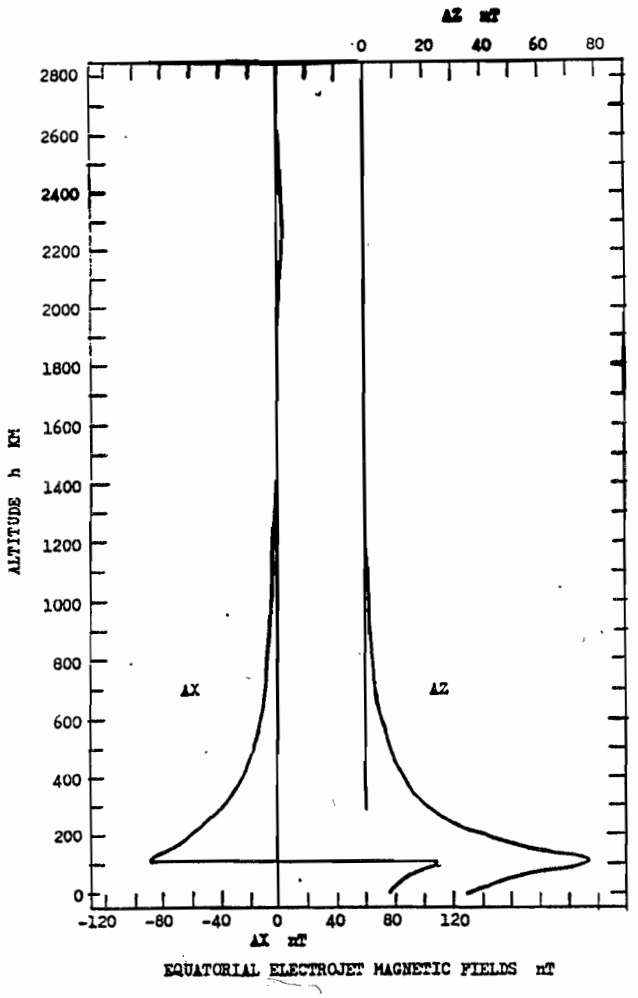

Fig. 2 Altitude profiles of the northward magnetic field ΔX and downward vertical field ΔZ of the equatorial electrojet (external **plus internal**) at local noon for the constant latitude x = 1°S.

Normally, the observed raw POGO data decreases with altitude in the range of 400-720 km (Onwumechili and Agu 1980) in agreement with ΔX in Fig. 2 There are, however, several cases in which it tends to increase with altitude, in small altitude ranges of about 400-480 and 560-600 km. However, such short altitude ranges are not firmly steady. The altitude profiles of Magsat data are consistent with those of the POGO data (Ravat and Hinze 1993).

3.4 Longitudinal Component

To obtain the longitudinal profiles of the magnetic fields of the equatorial electrojet (EEJ) the local noon values of the parameters ½k, a, α, b and β are put into Eqs. (3) and (4) for ΔX and ΔZ respectively, for each of the 36 selected longitudes. Because of space considerations we have not given the 36x5 = 180 values of parameters used. Being for the ground, v = 106 km is held constant. Three landmark magnetic values ΔX_o, ΔX_m, and ΔZ_M are calculated for each longitude, using u_o = 0, u_{mX} and u_M respectively. The resulting longitudinal profiles are given in Fig. 3.

The longitudinal profiles of ΔX_o, and ΔZ_M have peaks at about 95°E and 295°E longitudes and troughs at about 145°E and 240°E plus a broad trough from about 340°E to 60°E. This longitudinal variation is in good agreement with but better defined than Onwumechili et al. (1989) from thin current shell modelling. It is also in accord with the longitudinal profiles of raw satellite EEJ magnetic data of Cain and Sweeney (1972, 1973) from POGO satellites and Ravat and Hinze (1993) from Magsat.

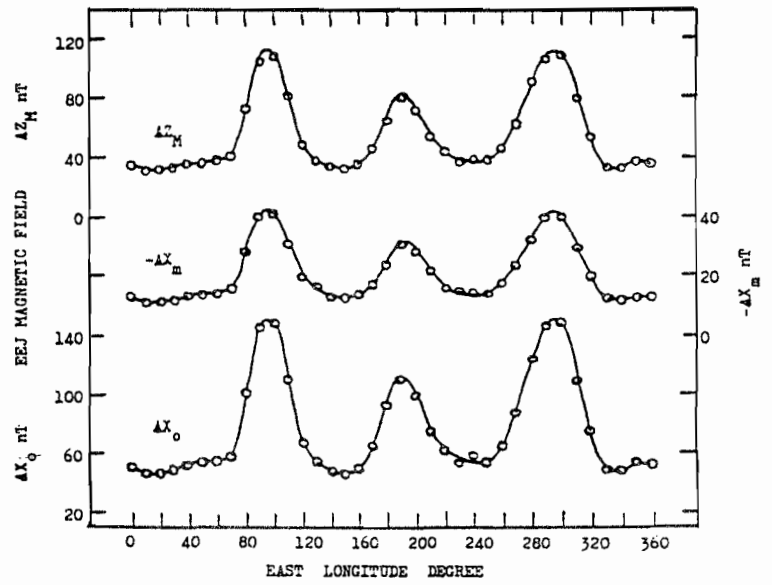

Fig. 3 Longitudinal profiles of the equatorial electrojet (EEJ) peak northward magnetic field ΔX_o at the dip equator, the peak southward field ΔX_m near the latitude of the peak return current on the flanks of the dip equator, and the peak downward vertical filed ΔZ close to the focus of the EEJ produced at local noon by the overhead EEJ current.

4 LONGITUDE-LOCAL TIME CROSS SECTION

The cross section is obtained for the ground surface at a fixed latitude. Therefore the fixed values of x = -1°, z = 106 km are put into Eqs. (1) and (2) for ΔX and ΔZ respectively. For each of the 36 selected longitudes λ, the values of the parameters ½k, a, α, b and β for each of the 7 local time hours t are put into Eqs. (1) and (2) to calculate ΔX and ΔZ respectively for the point (t, λ). Obviously, the 36x7x5 = 1260 values of the parameters used cannot be given here. After combining the external and internal fields at each point (t, λ), the resulting ΔX and ΔZ are arranged in a matrix table of 36 longitude rows and 7 local time hour columns. These are interpolated and joined for chosen contours.

The longitude-local time cross sections of the external plus internal EEJ ΔX and ΔZ are shown in Fig. 4(a) and Fig. 4 (b) respectively. At a fixed longitude the field peaks at local noon in accordance with section 3.1. And at a fixed local time, the fields peak at about 100°E, 190°E and 290°E with troughs between them as expected from section 3.4. Accordingly, three contour cells of high values appear. For ΔX the peaks of the contour cells are 122 nT at (12h, 100°E), 103 nT at (12h, 190°E) and 133 nT at ((12h, 290°E) but for ΔZ the peaks are 52 nT at (12h, 100°E), 44 nT at (12h, 190°E) and 57 nT at (12h, 290°E). When the fixed values of u and v are smaller than 1° and 106 km respectively the pattern remains the same but the values of the contours for ΔX are larger and conversely. For ΔZ the effect is the same for changes in v. For changes in u, the ΔZ contour values increase from near zero at u = 0 to a maximum at u = u_M before decreasing beyond u_M.

5 ALTITUDE-LOCAL TIME CROSS SECTION

The altitude-local time cross section is determined for the fixed latitude x = -1° using Eqs. (5) and (6). For each local time t the all longitude means of the parameters ½k, a, α, b and β appropriate for t are inserted into Eqs. (5) and (6). Because of space the 35 values of the parameters used for t = 9, 10, 11, ..., 15 hr are not given here. The fields, external and internal, are calculated for each selected altitude h and are combined for each point (t, h). These are arranged in a matrix table of h rows and t columns. They are interpolated for chosen contours, plotted and joined. The resulting altitude-local time cross sections for EEJ ΔX and ΔZ are given in Fig. 5(a) and Fig. 5 (b) respectively.

The basic difference between the cross sections of ΔX and ΔZ is caused by the change of sign of ΔX across the altitude h_e = 106 km of EEJ centre. In each cross section, at a fixed altitude

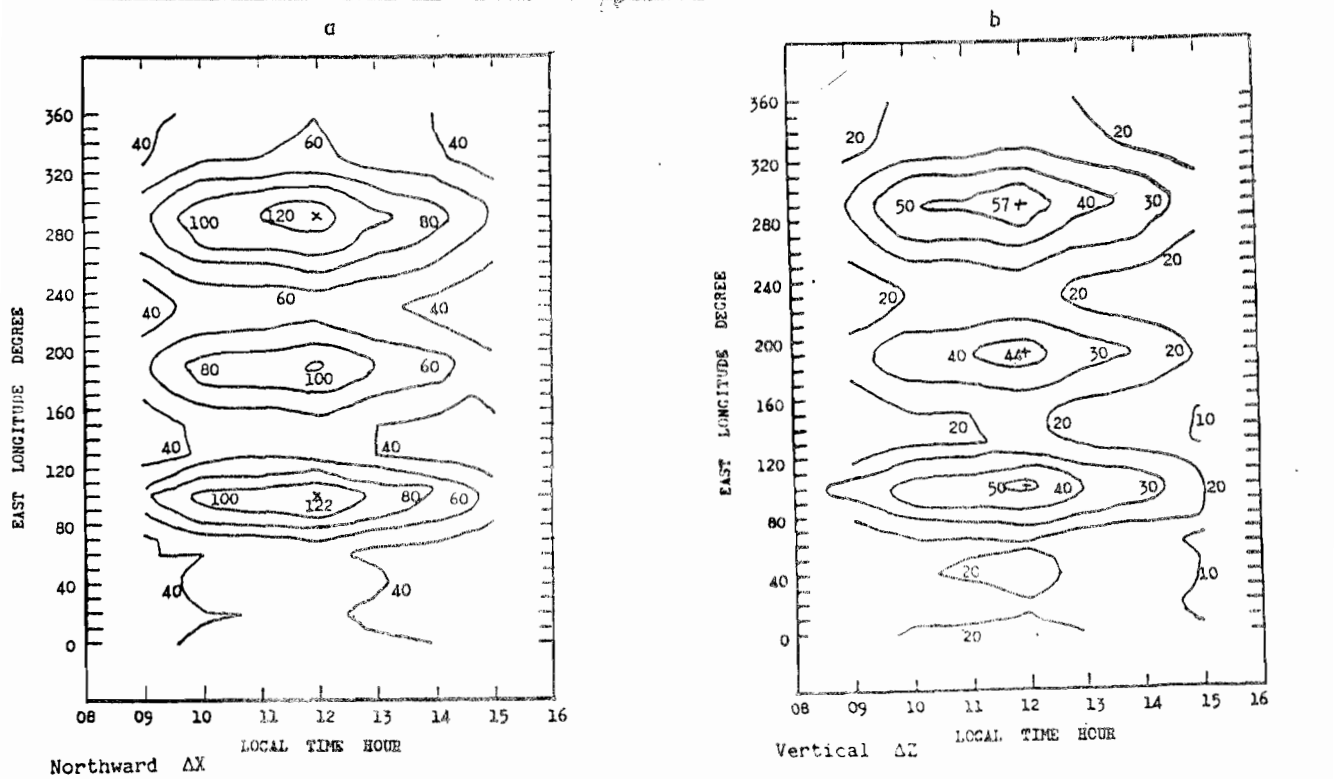

Fig. 4 Longitude-local time cross sections of equatorial electrojet magnetic fields (external plus internal)

(a) The northward field ΔX nT, showing contours of 100, 80, 60, and 40 nT. The crosses show local noon maxima of 122 nT, 103 nT and 133 nT at longitudes 100°E, 190°E and 290°E respectively.

(a) The downward vertical field ΔZ nT, showing contours of 50, 40, 30, 20 and 10 nT. Crosses indicate local noon maxima of 52 nT and 57 nT at longitudes of 100°E, 190°E and 290°E respectively.

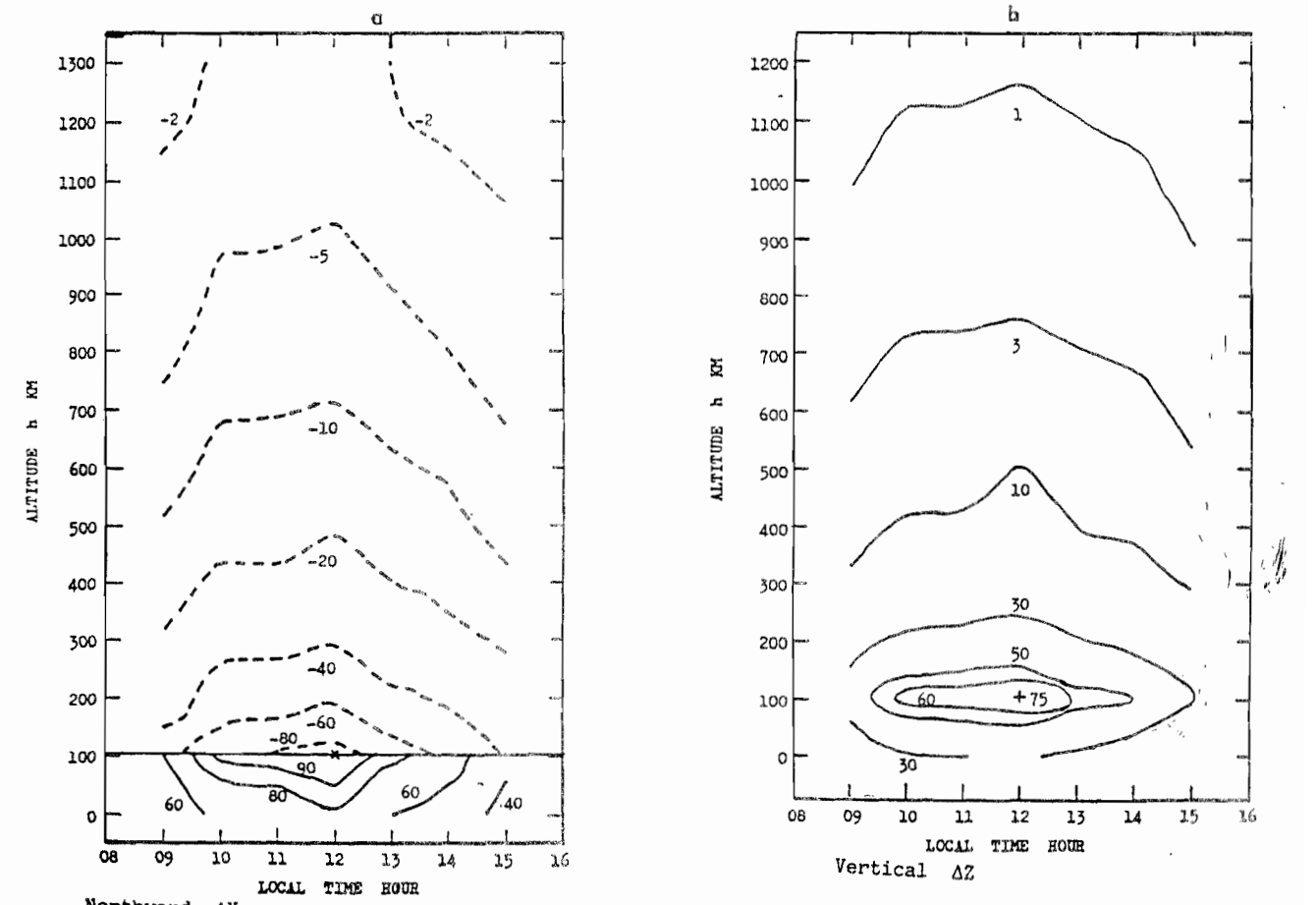

Fig. 5 Altitude-local time cross sections of all longitude means of equatorial electrojet magnetic fields (external plus internal).

(a) The northward field ΔX nT, showing contours of 90, ± 80, ± 60, -40, -20, -10, -5 and –2 nT. The cross shows local noon peak of 109 nT on the lower and –88 nT on the upper side of the current centre at 106 km altitude. Solid contours for positive ΔX and broken contours for negative ΔX.

(b) The downward vertical field ΔZ nT, showing contours of 60, 50, 30, 10, 3 and 1 nT. The cross marks the local noo

the field peaks at local noon as expected from section 3.1. At a fixed local time, each field varies with altitude as described in section 3.3. Accordingly, only one contour cell of high value is formed at the altitude of h_e = 106 km. At the point (12h, 106 km) the ΔX cell has a peak of 109 nT on the lower side and −88 nT on the upper side of the centre, while ΔZ has a peak of 75 nT. When the fixed latitude u is decreased the pattern remains the same but the contour values for ΔX increase and conversely. For ΔZ the pattern remains the same but the contour values increase as u increases from zero through maximum contour values at $u = u_M$. But beyond u_M the contour values decrease.

6 LATITUDE-LOCAL TIME CROSS SECTION

The latitude-local time cross section is set on the earth's surface by fixing the altitude h = 0 and z = 106 km. The external and internal parts of the EEJ fields are calculated at selected latitudes x, by inserting into Eqs. (3) and (4) the all longitude means of the parameters ½k, a, α, b and β appropriate for each hour t = 9, 10, ..., 15 hr. Thus 35 values of the parameters are used in all. The external and internal parts of the fields at the points (t, x) are combined and organized into a matrix table of x rows and t columns. The values are then interpolated for chosen contours and joined. The resulting latitude-local time cross sections are displayed in Fig. 6 (a) and Fig. 6 (b) for EEJ ΔX and ΔZ respectively.

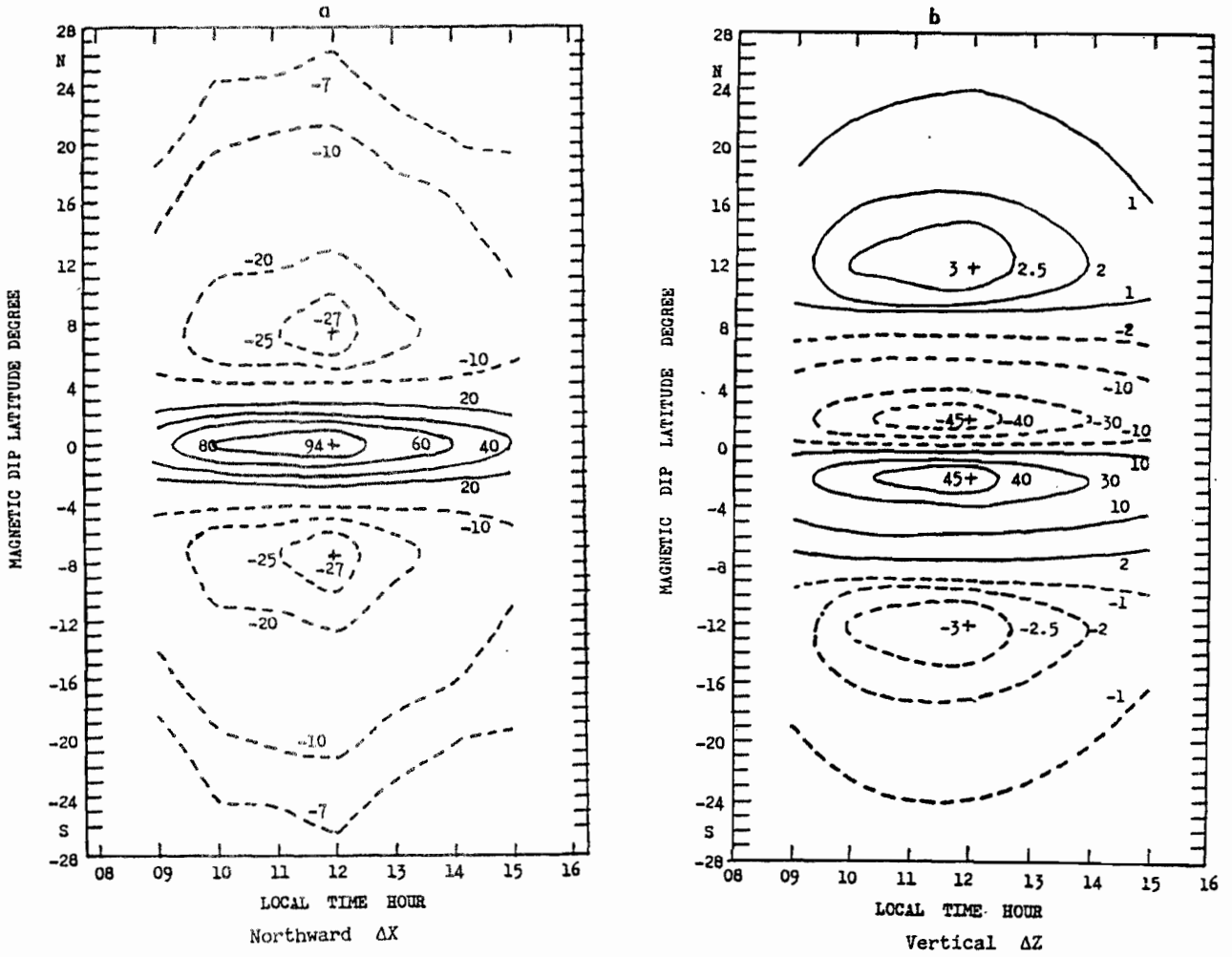

Fig. 6 Latitude-local time cross sections of all longitude means of equatorial electrojet magnetic fields (*external plus internal*). Solid contours for positive and broken contours for negative magnetic fields.

(a) The northward field ΔX nT, showing contours of 80, 60, 40, -25, ± 20 and ±10 nT. The crosses mark local noon peak of 94 nT and −27 nT at 0° and about ± 7.5° dip latitude respectively.

(b) The downward vertical field ΔZ nT, showing contours of ± 40, ± 30, ± 10, ± 2.5, ± 2 and ± 1 nT. The crosses indicate local noon maxima and minima of ± 45 nT at about ± 2° and ± 3 nT at about ± 12° dip latitude.

At any fixed latitude the magnitudes of the fields increase from morning to a peak at local noon and then decrease in accordance with section 3.1. As described in section 3.2, at a fixed local time, ΔX decreases from its peak ΔX_o at the dip equator to zero at its focus of about $w_X = 3.57°$ before decreasing to a minimum at $u_{mX} = 7.5°$. On the other hand, at a fixed local time ΔZ decreases to the north and increases to the south from near zero ΔZ_o at the dip equator. The magnitude reaches a peak at about $u_M = 2°$ before decreasing to zero at its focal latitude of about $w_Z = 8.2°$ from where it increases to a very small maximum at bout $u_{Mz} = 12°$ dip latitude.

The combination of local time and latitudinal variations creates three contour cells of ΔX: one of positive values and two of negative values; and four contour cells of ΔZ two of positive values and two of negative values. The contour cells of ΔX have peaks of 94 nT at (12h, 0°) and −27 nT at (12h, ± 7.5°). The contour cells of ΔZ have peaks of ± 45 nT at about (12h, ± 2°) and ± 3 nT at about (12h, ± 12°). The patterns remain the same but the contour values increase or decrease according as the ½k or j_o is greater or less than the value used in this case.

7 ALTITUDE-LONGITUDE CROSS SECTION

The altitude-longitude cross sections of EEJ magnetic fields are produced for the constant dip latitude x = -1°. For selected values of altitude $h = h_e - z$, the daytime mean values of the parameters ½k, a, α, b and β appropriate for a given longitude $\lambda = 0°, 10°, 20°, \ldots, 350°E$ are put into Eqs. (5) and (6) for ΔX and ΔZ respectively. Therefore a total of 36x5 = 180 values of the

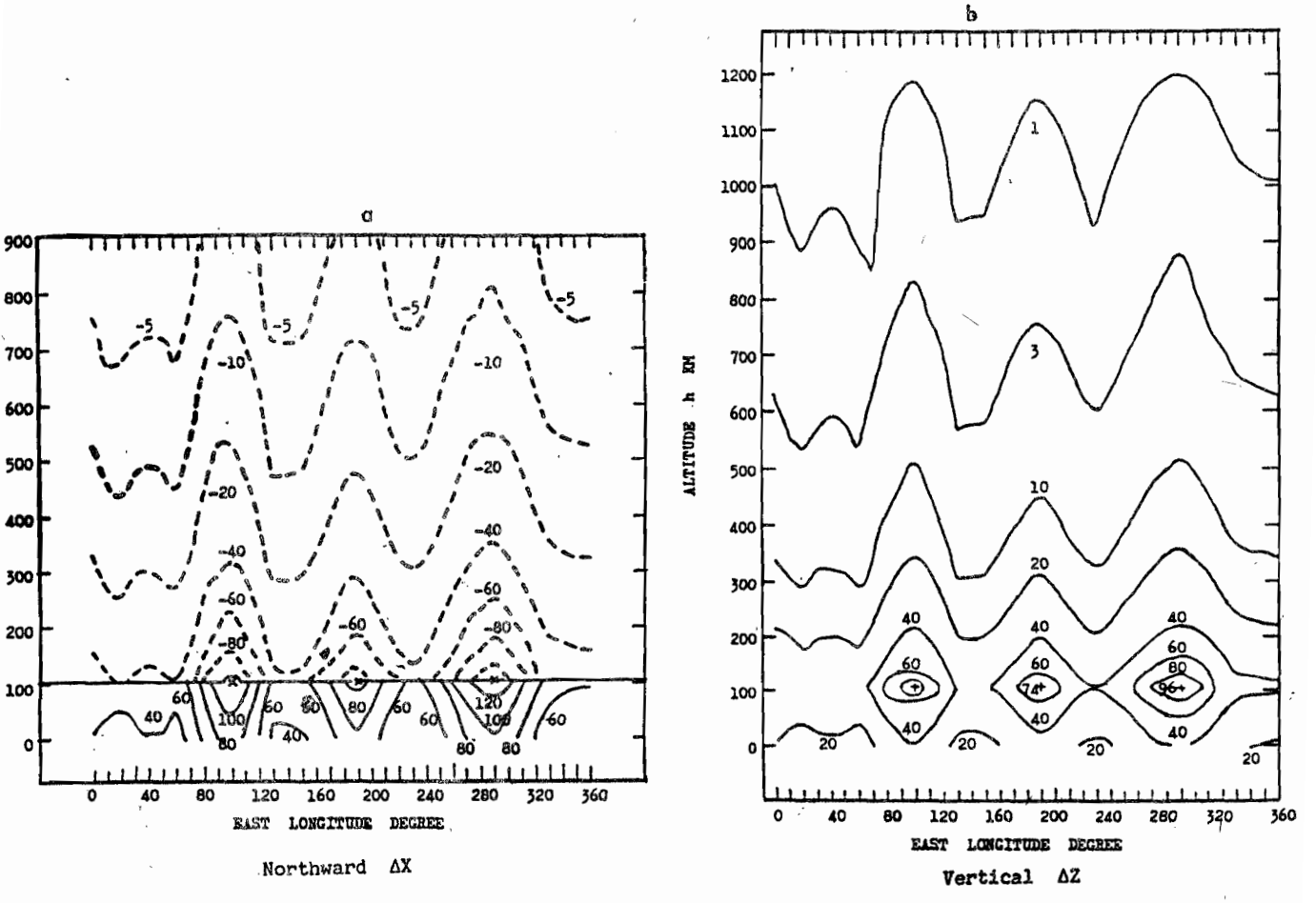

Fig. 7 Altitude-longitude cross sections of daytime means of equatorial electrojet magnetic fields (external plus internal).

(a) The northward field ΔX, nT, showing contours of 120, ± 100, ± 80, ± 60, ± 40, -20, -10 and −5 nT. The crosses mark positive peaks on the lower side and negative peaks on the upper side of the altitude of current centre at 106 km: (128 and −103 nT), (108 and −87 nT) and (140 and −113 nT) at longitudes of 100°E, 190°E and 290°E respectively.

(b) The downward vertical field ΔZ nT, showing contours of 80, 60, 40, 20, 10, 3 and 1 nT. Crosses show the maxima of 88 nT, 74 nT and 96 nT at 106 km altitude of the current centre at 100°E, 190°E and 290°E longitudes respectively.

parameters are used. Similarly, the internal fields are calculated for the same points (λ, h). After combining the external and internal parts of the fields, ΔX and ΔZ are arranged in their respective matrix tables of h rows and λ columns. The values are interpolated and plotted for chosen contours. The altitude-longitude cross sections of EEJ ΔX and ΔZ are shown in Fig. 7 (a) and Fig. 7 (b) respectively.

Along each longitude, ΔX and ΔZ vary with altitude as described in section 3.3 with ΔX changing sign at the altitude h_e of the current centre. At any fixed altitude, ΔX and ΔZ vary with longitude as described in section 3.4, reaching peaks at 100°E, 190°E and 290°E longitudes. The combined altitudinal and longitudinal variations form three contour cells of ΔX and three contour cells of ΔZ at the altitude h_e of the current centre. The peaks of the contour cells of ΔX are: 128 nT on the lower side and −103 nT on the upper side at (100°E, 106 km), and 140 nT on the lower side and −113 nT on the upper side at (290°E, 106 km). The peaks of the ΔZ contour cells are 88 nT at (100°E, 106 km), 74 nT at (190°E, 106 km), and 96 nT at (290°E, 106 km). The patterns of the cross sections remain the same, but the contour values increase or decrease according as ½k or j_o is greater or less than the daytime mean used here.

8 LATITUDE-LONGITUDE CROSS SECTION

The latitude-longitude cross sections of EEJ ΔX and ΔZ are set on the earth's surface by fixing the altitude h = 0, z = 106 km. For selected values of latitude x the daytime means of the

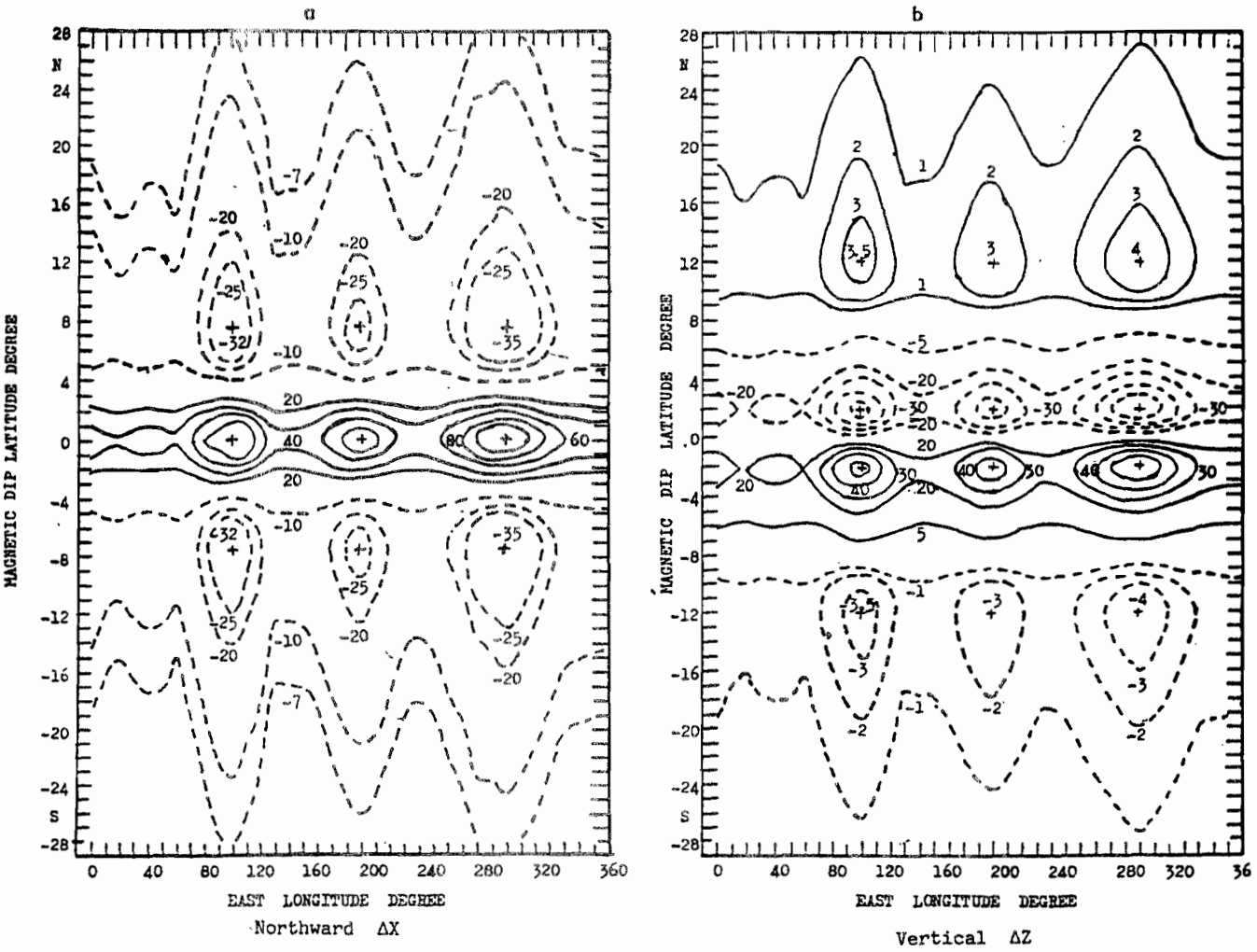

Fig. 8 Latitude-longitude cross sections of daytime means of equatorial electrojet magnetic fields (external plus internal). Solid contours for positive and broken contours for negative magnetic fields.

(a) The northward field ΔX nT, showing contours of 100, 80, 60, - 40, 25, ± 20 -10 and -7 nT. At longitudes of 100°E 190°E, and 290°E crosses mark peaks of 110 nT, 93 nT and 120 nT respectively at the dip equator and of -32 nT, -27 nT and -35 nT respectively at about ± 7.5° dip latitude.

(b) The downward vertical field ΔZ nT, showing contours of ± 50, ± 40, ± 30, ± 20, ± 5 ±3, ± 2 ± 1 nT. At longitudes of 100°E, 190°E and 290°E, crosses mark maxima and minima of ± 53 nT ± 45 nT and ±58 nT respectively at about ± 2° and of ± 3. 5nT, ± 3 nT and ± 4 nT respectively at about ± 12 dip latitude

parameters ½k, a, α, b and β appropriate for each longitude λ = 0°, 10°, 20°, ..., 350°E are inserted into Eqs. (3) and (4) for ΔX and ΔZ respectively. Similarly, the internal fields are calculated for the same points (λ, x). The results of combining the external and internal parts of the fields are then organized in matrix tables of x rows and λ columns. By interpolation, the chosen contours are drawn. The latitude-longitude cross sections of EEJ ΔX and ΔZ are displayed in Fig. 8 (a) and 8 (b) respectively.

These beautiful cross sections look complex but they can be easily understood from section 3. Along any fixed latitude the fields vary with longitude in accordance with section 3.4 reaching peaks at 100°E, 190°E and 290°E. Along any fixed longitude the fields vary with latitude as described in section 3.2. The landmark distances of ΔX are u_{oX} = 0° (maximum ΔX), w_X = ± 3.6° (zero ΔX), and u_{mX} = ± 7.5° (minimum ΔX) . The landmark distances for ΔZ are u_{oZ} = 0° (about zero ΔZ), u_M = ± 2° (minimum/maximum ΔZ) w_Z = ± 8.2° (zero ΔZ), and u_{mZ} = ± 12° (minimum/maximum ΔZ). The combination of the latitudinal and longitudinal variations produce for ΔX three positive and six negative contour cells, and for ΔZ six positive and six negative contour cells.

The ΔX positive contour cell peaks are 110 nT at (100°E, 0°), 93 nT at (190°E, 0°) 120 nT at (290°E, 0°) and its negative peaks are - 32 nT at (100°E, ± 7.5°), -27 nT at (190°E, ± 7.5°) and -35 nT at (290°E, ± 7.5°). The peaks of the ΔZ contour cells are ± 53 nT at (100°E, ± 2°), ± 45 nT at (190°E, ± 2°) and ± 58 nT at (290°E, ± 2°), before its focus and ± 3.5 nT at (100°E, ±12°), ± 3 nT at (190°E, ±12°) and ± 4 nT at (290°E, ±12°) beyond its focus.

9 ALTITUDE-LATITUDE CROSS SECTION

The altitude-latitude cross sections of EEJ ΔX and ΔZ are determined for local noon conditions. For selected values of altitude h = h_e – z = 0, 56, 106, 156, 212, 256, 306, 406, 506, ..., 1006 km, the all longitude local noon means of the parameters ½k, a, α, b and β are inserted into Eqs. (1) and (2) for ΔX and ΔZ respectively with a fixed value of latitude x°. This is repeated for latitudes x = 0°, ± 1°, ± 2°, ± 3°, ..., ± 28°. Similarly, the internal fields are determined at the same points (x, h). For each component, the result of combining the external and internal fields at each point are organized into a matrix table of h rows and x columns. The desired contours are interpolated and plotted. The altitude-latitude cross sections of EEJ ΔX and ΔZ are displayed in Fig. 9 (a) and Fig. 9 (b) respectively.

These cross sections are not as simple as others but the general principles still apply. At a fixed latitude the fields still vary with altitude in accordance with section 3.3. At any fixed altitude except the altitude of the current centre h_e, the fields vary with latitude as described in section 3.2. the fields vary with latitude as described in section 3.2. In particular, the peaks and landmark distances on the earth's surface are the same as given for local noon in section 6. One of the striking features of the cross sections is the change in sign of ΔX across the altitude h_e = 106 km and the change in sign of ΔZ across the latitude x = 0°. This has important implications for the peaks and landmark distances of ΔX at the altitude h_e = 106 km.

Because the external ΔX_e changes sign but the internal ΔX_i does not change sign across h_e, their combination is

$$\Delta X = \Delta X_e + \Delta X_i \text{ below } h_e, \quad \text{10a}$$
$$\Delta X = -\Delta X_e + \Delta X_i \text{ above } h_e, \quad \text{10b}$$

Consequently:

(a) There is a jump discontinuity with ΔX peaks larger on the lower side of h_e than on the upper side of h_e

(b) Arising from (a), with the exception of u_{oX} = 0°, the landmark distances are greater on the lower side of h_e than on the upper side of h_e.

(c) Arising from (a) and (b) the contours of ΔX are not closed curves.

On the lower side of h_e = 106 km, ΔX has a central positive peak of 151 nT at u_{Ox} = 0°, zero values at about w_X = ± 2.9°, and negative peaks of -33 nT at u_{MX} = 6° dip latitude. But on the upper side of h_e, ΔX has a central negative peak of –128 nT at u_{Ox} = 0°, zero values at about w_X = ± 2.7°, and positive peaks of 31 nT at about u_{MX} = 5° dip latitude.

In general, with the exception of the central u_o, the landmark distances of both ΔX and ΔZ

increase as the altitude increases above or decreases below the altitude of the centre h_o. However, for ΔZ the increase is slow within about 100 km of h_o and thereafter the increase becomes faster. Also the increases are faster above h_o than below h_o. Arising from these, the differences between the landmark distances of ΔZ on h_o level and on the ground are much smaller than the corresponding differences for ΔX. Consequent on the general phenomenon, with the exception of the central altitude peaks, the peak altitudes of the contours increase progressively with their latitudes above h_o. But below h_o, as the peak altitudes of the contours progressively decrease, their latitudes increase.

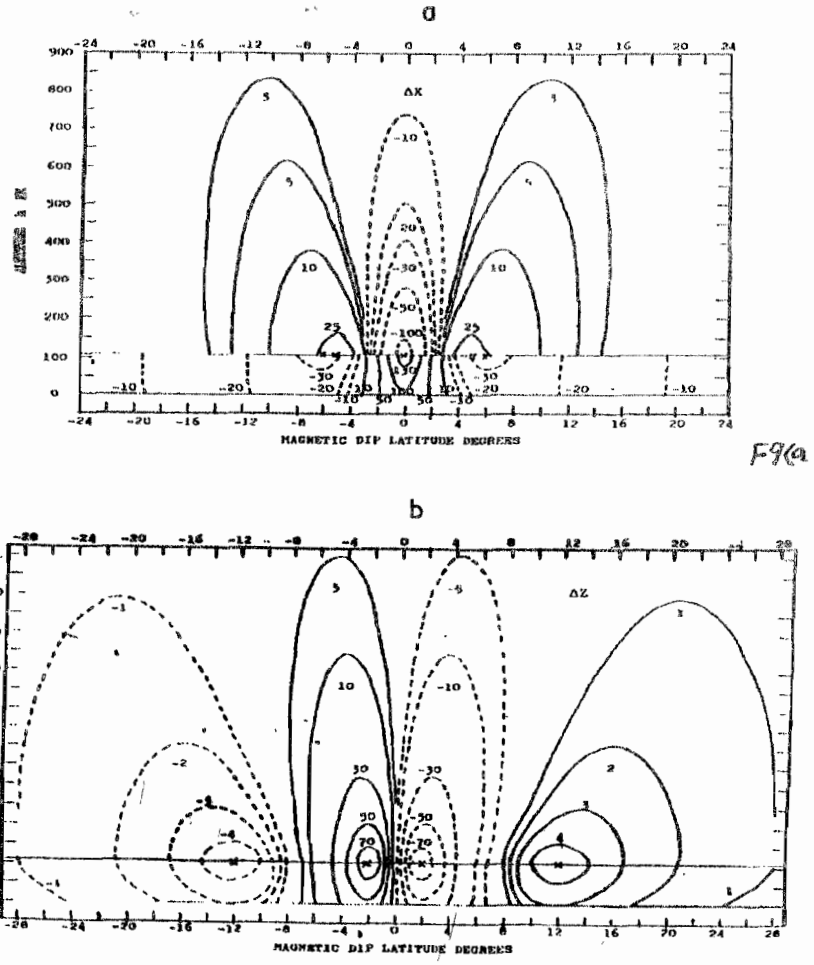

F-9(a)

Fig. 9 Altitude-latitude cross sections of all longitude means of local noon magnetic fields of equatorial electrojet (external plus internal). Solid contours for positive and broken contours for negative fields.

(a) The northward field ΔX, nT, showing contours of 130, ± 100, ± 50, -30, 20, -25, ±10, -5 and 3 nT. Crosses mark positive peaks on the lower side and negative peaks on the upper side of the altitude of current centre at 106 km: 151 nT and –128 nT at 0°, 31 nT at about ± 5°, -33 nT at about ± 6° dip latitude.

(b) The downward vertical field ΔZ nT, showing contours of ±70, ±50, ±30, ±10, ±5, ±4, ±3 ±2 and 1 nT. At the altitude of the current centre h = 106 km, the crosses mark the maxima and minima of ±89 nT at about ±1.5°, and of ±5 nT at about ± 12° dip latitude.

10 DISCUSSIONS

We first discuss the physical mechanisms responsible for the components of the four-dimensional variations of EEJ magnetic fields before discussing the cross section. The local time variation of EEJ ΔX from the POGO data very much resembles the local time variations of EEJ peak current intensity J_o derived from the POGO data (Agu and Onwumechili 1981, Ozoemena and

Onwumechili 1988) as well as the EEJ current intensity derived from Indian observatories data (Oko et al. 1996). There is no doubt that this current intensity is responsible for the variations of the magnetic fields. The local time variation arises from the solar control of electric field and conductivity through plasma density in the E-region of the ionosphere where EEJ flows.

For observational evidence on the source of the altitude component of the variation, we turn to rocket measurements of ionospheric currents. Over 60% of rockets flown within 0° to 2° dip latitude found two current layers peaking at 106 ± 1 km and 136 ± 8 km altitudes respectively (Onwumechili 1992a, b). The numerical model calculations of Takeda and Maeda (1980, 1983) and Singh and Cole (1987) also have indications of two current layers. Judging from the characteristics of the two layers, the lower current layer is the EEJ and the upper current layer is the worldwide part of Sq (WSq) (Onwumechili 1992b). Moreover, the vertical Hall polarization electric field E_z which drives the major part of EEJ was measured by Sartiel (1977) near local noon at Thumba close to the dip equator. The E_z peaked at about 101 km and decreased to zero at about 115 km altitude. This confirms that the lower current layer is the EEJ.

The altitude parameters of EEJ derived from rocket data in India and Peru have been successfully compared with those of the POGO data used in this paper (Onwumechili 1997 section 3.12). The altitude variation of the current dehsity of EEJ (lower) current layer controls the altitude variation of EEJ ΔX and ΔZ.

It has already been shown in section 3.2 that the latitudinal variation of EEJ ΔX and ΔZ from the POGO data agrees very well with the observations on the earth's surface. One of the remarkable features of this latitudinal variations is the depressed shoulders of ΔX on the ground. On the POGO satellites, the depressed shoulders reverse into high shoulders (Cain and Sweeney 1972, 1973). This shows that it is caused by westward currents in the ionosphere between the ground and the satellites. The depressed shoulders on the ground have been observed by Hutton (1967), Fambitakoye and Mayaud (1976) and Hesse (1982), and has been successfully modelled by Anandarao and Raghavarao (1987). Of particular significance is the finding of Hesse (1982) that the depressed shoulders are permanently connected with the EEJ. They increase and decrease with the EEJ. They are absent when the EEJ is absent and they reverse when the EEJ reverses into counter electrojet. It is therefore natural to conclude that the westward current causing the depressed shoulders is part of the return current of the eastward EEJ current.

Onwumechili (1996) produced the current vortex of the EEJ (lower) current layer from observational data in India. In view of Stening (1995) he gave the electric fields that drive all the parts of the EEJ vortex. With the parameters from the POGO data used here, he demonstrated that the return current of the EEJ which peaks at about 5. 18 ± 0. 09° dip latitude, exactly annuals the forward current within the latitudinal extent of EEJ of about 12° dip latitude. The numerical models of Sugiura and Poros (1969), Anandarao and Raghavarao (1979), Takeda and Maeda (1983), Singh and Cole (1987), and Raghavarao and Anandarao (1987) have found the westward part of the EEJ current in the neighbourhood of the latitude of its peak.

Rockets have observed the eastward (forward) component of EEJ current vortex in the region of 0° – 2° dip latitude and the westward (return) current component of the vortex close to 5° dip latitude (Onwumechili 1992a, b). Rastogi (1996) has produced evidence of the north-south component of the EEJ current vortex from observational data. The current vortex of EEJ, confined within about ± 15° dip latitude, is therefore strongly supported by observations. It is this current vortex that accounts for the latitudinal variation of EEJ magnetic fields. It is well known that ΔX resembles the eastward current intensity J causing it. Accordingly, ΔX is a maximum at the dip equator where the current intensity is maximum; the $\Delta X = 0$ at about 3.6° shortly after $J = 0$ at its focus near 2.76°; and ΔX is a minimum at about 7.5° following the minimum of J at about 5.18° dip latitude. Onwumechili et al. (1989) have explained why the latitudes of the focus and minimum of ΔX are somewhat higher than those of the current intensity J.

The longitudinal variation of EEJ magnetic fields in section 3.4 follows the longitudinal variations of EEJ peak current density J_o and total forward current I_F in Onwumechili and Agu (1981), Ozoemena and Onwumechili (1987), Onwumechili et al. (1989), and is consistent with the variation of I_F in Deminov et al. (1988). It is however inconsistent with Sugiura and Poros (1969) most likely because they assumed that the eastward electric field E_y is independent of longitude. But the AE-E satellite discovered that on the average, the electric field E_y is proportional to the ambient magnetic field B within about ± 10° dip latitude (Coley et al. 1990). It follows that EEJ current density j is given by

$$j = \sigma_3 E_y = C\sigma_3 B \quad \ldots\ldots 11$$

where C is the constant of proportionality and σ_3 is the effective conductivity. Therefore the

longitudinal peak of EEJ current and magnetic fields at 100°E arises from maximum B there, their peak at 290°E comes from the maximum σ_3 there and their peak at 190°E may be explained by the combination of B and σ_3 values at that longitude.

Each cross section is made up of two of the four components whose physical mechanisms have been discussed. Therefore, we have already covered the basic physical mechanisms of all the cross sections. In each cross section, the peak of a contour cell occurs where both of the two components making up the cross section have their maximum magnitudes at the same point.

The only cross section we know in literature is Doumouya's latitude-local time cross section of the combined fields of EEJ plus WSq confined within about ± 5° dip latitude. The contour of (EEJ ΔX + WSq ΔX) cannot show where EEJ $\Delta X = 0$ unless the two are plotted separately as in Fig. 1 (b). His latitude range of ± 5° is too short to show EEJ ΔX_m at about $u_{mX} = 7.5°$ dip latitude. However, his ΔH contour cell is very much like our ΔX positive contour cell in Fig. 6 (a). Within the limits of his latitude range, his cross section of ΔZ is in good agreement with ours in Fig. 6 (b). In particular, the peaks of his contour cells occur at $u_M = 2.5° \pm 0.2°$ on both sides of the dip equator as compared with 2.1° here. Indeed, his u_M is expected to be somewhat larger because the continued increase of WSq ΔZ is expected to increase his u_M for (EEJ ΔZ + WSq ΔZ) beyond the u_M for EEJ ΔZ alone.

The expectation that the cross sections of the EEJ magnetic fields will somewhat resemble the corresponding cross sections of the currents generating them is fully realized. The longitude-local time cross sections in Fig. 4 resemble the longitude-local time cross sections of EEJ current density j, intensity J and total forward current I_f. The altitude-local time cross section of ΔZ in Fig. 5 (b) resembles the altitude-local time cross section of EEJ current density j. The Fig. 5 (a) is marred by the change of sign of ΔX across the altitude h_e, but its halves above and below h_e resemble the j cross section. The latitude-local time cross section of ΔX in Fig. 6 (a) resembles the latitude-local time cross sections of EEJ current density j and intensity J. The cross section for ΔZ in Fig. 6 (b) is marred by the change of sign of ΔZ across $x = 0°$, but each half to the north and south resembles the current cross sections.

Similarly, the altitude-longitude cross section of ΔZ in Fig. 7 (b) and each half of Fig. 7(a) resemble the altitude-longitude cross sections of current density j. Also the latitude-longitude cross section of ΔX in Fig. 8 (a) and each half of Fig. 8 (b) resemble latitude-longitude cross section of EEJ current density j and intensity J. Finally, allowing for the change of sign of ΔX across the altitude h_e and the change of sign of ΔZ across the latitude $x = 0°$, the upper and lower halves of Fig. 9 (a) for ΔX, and the north and south halves of Fig. 9 (b) for ΔZ resemble their corresponding cross section of EEJ current density j. They may be compared with the cross section of j in Anandarao and Raghavargo (1979) and Raghavarao and Anandarao (1987).

As the longitude increases from 0° to 100°E, the values of ΔX and ΔZ increase to their peaks at 100°E. Thereafter, their values decrease to their troughs at about 145°E. Further on, they again increase to peaks at 190°E, decrease to troughs at about 240°E and increase to another peak at 290°E. That accounts for the wavy nature of the cross sections involving longitude.

11 CONCLUSIONS

The POGO series of satellites measured the four-dimensional variation of the equatorial electrojet (EEJ) magnetic field in certain ranges of local time, altitude, latitude and longitude in over 2000 traversals across the EEJ from 1967 to 1969. Analysis of the enormous quantity of data with a thick current shell model produced 894 values of certain parameters capable of generating the variations of EEJ ΔX and ΔZ with local time, altitude, latitude, and longitude. They agree with the best available observations of these variations.

Twelve cross sections for ΔX and ΔZ have been composed by taking two components of the variations at a time leading to: longitude-local time, altitude-local time, latitude-local time, altitude-longitude, latitude-longitude and altitude-latitude cross sections of each of EEJ ΔX and ΔZ. In each cross section, the peak of a contour cell occurs where both of the two components making up the cross section have their maximum magnitudes at the same point. The peak values and locations of the contour cells in each cross section have been given.

The expectation that the cross sections of EEJ magnetic fields will somewhat resemble the corresponding cross sections of the currents generating them has been fully realized. The physical mechanisms responsible for each of the four components of the variations and therefore of the cross sections have been discussed.

REFERENCES

Agu, C.E. and Onwumechili, C.A., 1981. Temporal variations of POGO equatorial electrojet parameters, J. Atmos. Terr. Phys., 43: 809-816.

Anandarao, B.G and Raghavarao, R., 1979. Effects of vertical shears in the zonal kinds on the electroject, Space Res., XIX: 283 – 286.

Cain, J.C. and Sweeney, R.E., 1972. POGO Observations of the Equatorial Electrojet, Godard Space Flight Center Publications, X-645-72-299, 54 pp.

Cain, J.C. and Sweeney, R.E., 1973. The POGO data, J. Atmos. Terr. Phys., 35: 1231-1247.

Coley, W.R., McClure, J.P. and Hanson, W.B., 1990. Equatorial fountain effect and dynamo drift signatures from AE-E observations, J. Geophys. Res., 95: 1845-21290.

Davis, T.N., Burrows, K. and Stolarik, J.D., 1967. A latitude survey of the equatorial electrojet with rocket-borne magnetometers, J. Geophys. Res., 72: 1845 – 1861.

Deminov, M.G., Kochenova, N.A. and Sitnov, Yu. S., 1988. Longitudinal variations of the electric field in dayside equatorial ionosphere, Geomagnetism and Aeronomy, 28: 57 – 60.

Doumouya, V., 1995. Etude des effects magnetiques de l'electrojet equatorial, Ph.D. Thesis, Universite Nationale de Cote d'Ivoire, 178 pp.

Fambitakoye, O. and Mayaud P.N., 1976. E quatorial electrojet and regular daily variation S_R – I. A determination of the equatorial electrojet parameters, J. Atmos. Terr. Phys., 38: 1-17.

Forbes, J.M., 1981. The equatorial electrojet, Rev. Geophys. Spae Phys., 19: 469 – 504.

Forbush, S.E. and Cassaverde, M., 1961. The Equatorial Electrojet in Peru, Carnegie Institution of Washington Publication, No. 620, 135 pp.

Hesse, D., 1982. An investigation of the equatorial electrojet by means of ground-based magnetic measurements in Brazil, Ann. Geophys., 38: 315-320.

Hutton, R., 1967. Sq current in the American equatorial zone during the IGY – I. Seasonal effects, J. Atmos. Terr. Phys., 29: 1411-1427.

Oko, S.O., Onwumechili, C.A. and Ezema, P.O., 1996. Geomagentically quiet day ionospheric currents over the Indian sector – II. Equatorial electrojet currents, J. Atmos. Terr. Phys., 58: 555-564.

Onwumechili, C.A., 1967. Geomagnetic variations in the equatorial zone, in Physics of Geomagnetic Phenomena vol. 1, Chap. III-2, 425-507, edited by Matsushita, S and Campbell, W.H., Academic Press, New York.

Onwumechili, C.A., 1992a. A study of rocket measurements of ionospheric currents – III. Ionoshperic currents at the magnetic equator, Geophys. J. Int., 108: 647-659.

Onwumechili, C.A., 1992b. A study of rocket measurements of ionospheric currents – IV. Ionospheric currents in the transition zone and the overview of the study, Geophys. J. Int., 108: 660-672.

Onwumechili, C.A., 1996. Spatial and temporal distributions of ionospheric currents in subsolar elevations, J. Atmos. Terr. Phys., in press.

Onwumechili, C.A., 1997. The Equatorial Electrojet, Gordon and Breach Science Publishers, Amsterdam.

Onwumechili, C.A., and Agu, C.E., 1981. Longitudinal variations of equatorial electrojet derived from POGO satellites observations, Planet. Space Sci., 29; 627-634

Onwumechili, C.A.. and Ezema, P.O., 1992. Latitudinal and vertical parameters of the equatorial electrojet from an autonomous data set, J. Atmos. Terr., Phys., 54; 1535-1544.

Onwumechili, C.A., Oko, S.O. and Ezema, P.O., 1996. Geomagnetically quiet day ionospheric currents over the Indian sector – I. Worldwide part of Sq currents, J. Atmos. Terri Phys., 58: 541 – 553.

Onwumechili, C.A., Ozoemena, P.C. and Agu, C.E., 1989. Landmark values of equatorial electrojet current and magnetic field along a meridian near noon, J. Geomag. Geoelectr., 41: 443-459.

Ozoemena, P.C. and Onwumechili, C.A., 1987. Global variations of the POGO electrojet parameters during the solstice, J. Geomag. Geoelectr., 39: 625-636.

Ozoemena, P.C. and Onwumechili, C.A., 1988. Diurnal variations of equatorial electrojet parameters derived from POGO solstitial data, J. Atmos. Terr. Phys., 50: 181-184.

Raghavarao, R. and Anandarao, B.G., 1987. Equatorial electrojet and counter electrojet, Indian J. Rad. Space Phys., 16: 54-75.

Rastogi, R.G., 1989. The equatorial electrojet: Magnetic and ionospheric effects, in, Geomagnetism vol. 3. 461-525, edited by Jacobs, J.A., Academic Press, London.

Rastogi, R.G., 1996. Solar flare effects on zonal and meridional currents at the equatorial electrojet station, Annamalainagar, J. Atmos. Terr. Phys., 58: 1413-1420.

Ravat, D. and Hinze, W.J., 1993. Considerations of variations in ionospheric field effects in mapping equatorial lithospheric Magsat magnetic anomalies, Geophys. J. Int., 113: 387-398.

Sartiel, J., 1977. Champs electriques la region de l'electrojet equatorial, Ph.D. Thesis, University of Paris VI, France.

Singh, A. and Cole, K.D., 1987. A numerical model of the ionospheric dynamo – III. Electric current at equatorial and low latitudes, J. Atmos. Terr. Phys., 49: 539-547.

Stening, R.J. 1995. What drives the equatorial electrojet? J. Atmos. Terr. Phys., 57: 1117-1128.

Sugiura, M. and Poros, J.D., 1969. An improved equatorial electrojet with a meridional current system, J. Geophys. Res., 74: 4025-4034.

Takeda, M. and Maeda, H., 1980. Three-dimensional structure of ionospheric currents – I. Currents caused by diurnal tidal winds, J. Geophys. Res., 85: 6895-6899.

Takeda, M. and Maeda, H., 1983. F-region dynamo in the evening – Interpretation of equatorial ΔD anomally found by MAGSAT, J. Atmos. Terr. Phys., 45: 401-408.